Heliyon 9 (2023) e20335

Contents lists available at ScienceDirect

Heliyon

journal homepage: www.cell.com/heliyon

Construction of 3D and 2D contrast-enhanced CT radiomics for prediction of CGB3 expression level and clinical prognosis in bladder cancer

Yuanfeng Zhang [a,f,1,2], Zhuangyong Xu [b,1,2], Shaoxu Wu [c], Tianxiang Zhu [d], Xuwei Hong [a], Zepai Chi [a], Rujan Malla [e], Jingqi Jiang [f], Yi Huang [c], Qingchun Xu [a], Zhiping Wang [f], Yonghai Zhang [a,*]

[a] Department of Urology, Shantou Central Hospital, Shantou, PR China
[b] Department of Radiology,Shantou Central Hospital, Shantou, PR China
[c] Department of Urology, Sun Yat-sen Memorial Hospital, Guangzhou, PR China
[d] Department of Cardiothoracic Surgery, Shantou Central Hospital, Shantou, PR China
[e] Department of Radiology, Nepal Medical Collage Teaching Hospital, Kathmandu, Nepal
[f] Department of Urology, Lanzhou University Second Hospital, Key Laboratory of Urological Disease of Gansu Province, Clinical Center of Gansu Province for Nephron-Urology, Lanzhou, PR China

ARTICLE INFO

Keywords:
Bladder cancer
Chorionic gonadotropin subunit beta
CT radiomics
Predictive models

ABSTRACT

Objective: The purpose of this study was to construct a 3D and 2D contrast-enhanced computed tomography (CECT) radiomics model to predict CGB3 levels and assess its prognostic abilities in bladder cancer (Bca) patients.
Methods: Transcriptome data and CECT images of Bca patients were downloaded from The Cancer Imaging Archive (TCIA) and The Cancer Genome Atlas (TCGA) database. Clinical data of 43 cases from TCGA and TCIA were used for radiomics model evaluation. The Volume of interest (VOI) (3D) and region of interest (ROI) (2D) radiomics features were extracted. For the construction of predicting radiomics models, least absolute shrinkage and selection operator regression were used, and the filtered radiomics features were fitted using the logistic regression algorithm (LR). The model's effectiveness was measured using 10-fold cross-validation and the area under the receiver operating characteristic curve (AUC of ROC).
Result: CGB3 was a differential expressed prognosis-related gene and involved in the immune response process of plasma cells and T cell gamma delta. The high levels of CGB3 are a risk element for overall survival (OS). The AUCs of VOI and ROI radiomics models in the training set were 0.841 and 0.776, while in the validation set were 0.815 and 0.754, respectively. The Delong test revealed that the AUCs of the two models were not statistically different, and both models had good predictive performance.
Conclusion: The CGB3 expression level is an important prognosis factor for Bca patients. Both 3D and 2D CECT radiomics are effective in predicting CGB3 expression levels.

* Corresponding author. Department of Urology, Shantou Central Hospital, Shantou, 515031, PR China.
E-mail address: zhang_yonghai@126.com (Y. Zhang).
[1] Yuanfeng Zhang and Zhuangyong Xu contributed equally to this work.
[2] These authors are co-first authors.

https://doi.org/10.1016/j.heliyon.2023.e20335
Received 1 June 2023; Received in revised form 12 September 2023; Accepted 19 September 2023
Available online 20 September 2023

1. Introduction

Bladder cancer (Bca) is the most popular malignant tumor of the urinary tract system as well as the fourth most popular cancer in men. The incidence of Bca ranks first among urological malignancies in China [1,2]. Despite some good results in the treatment of Bca in recent years, such as radical cystectomy combined with neoadjuvant chemotherapy and immunotherapy for muscle-invasive bladder cancer (MIBC), the 5-year survival rate for MIBC is still below 50% [1]. It is crucial that an early diagnosis and personalized therapy is the key to successful treatment. Although clinicopathological features, tumor antigens such as BTA, NMP22, and conventional imaging features can be used as prognostics, limitations such as low specificity and the need for tissue specimens obtained by invasive manipulation make it difficult to meet the clinical needs [3,4]. Therefore, developing a noninvasive method to predict the molecular heterogeneity of Bca and further assess the prognosis and risk of tumor recurrence accurately is a current clinical challenge.

It has been accepted that not alone gynecological cancers but additionally abounding added tumors of altered origins are able of secreting β-hCG [5,6]. The β-hCG mRNA expression of Bca has been reported to correlate with the tumor clinical stage. Tumors that

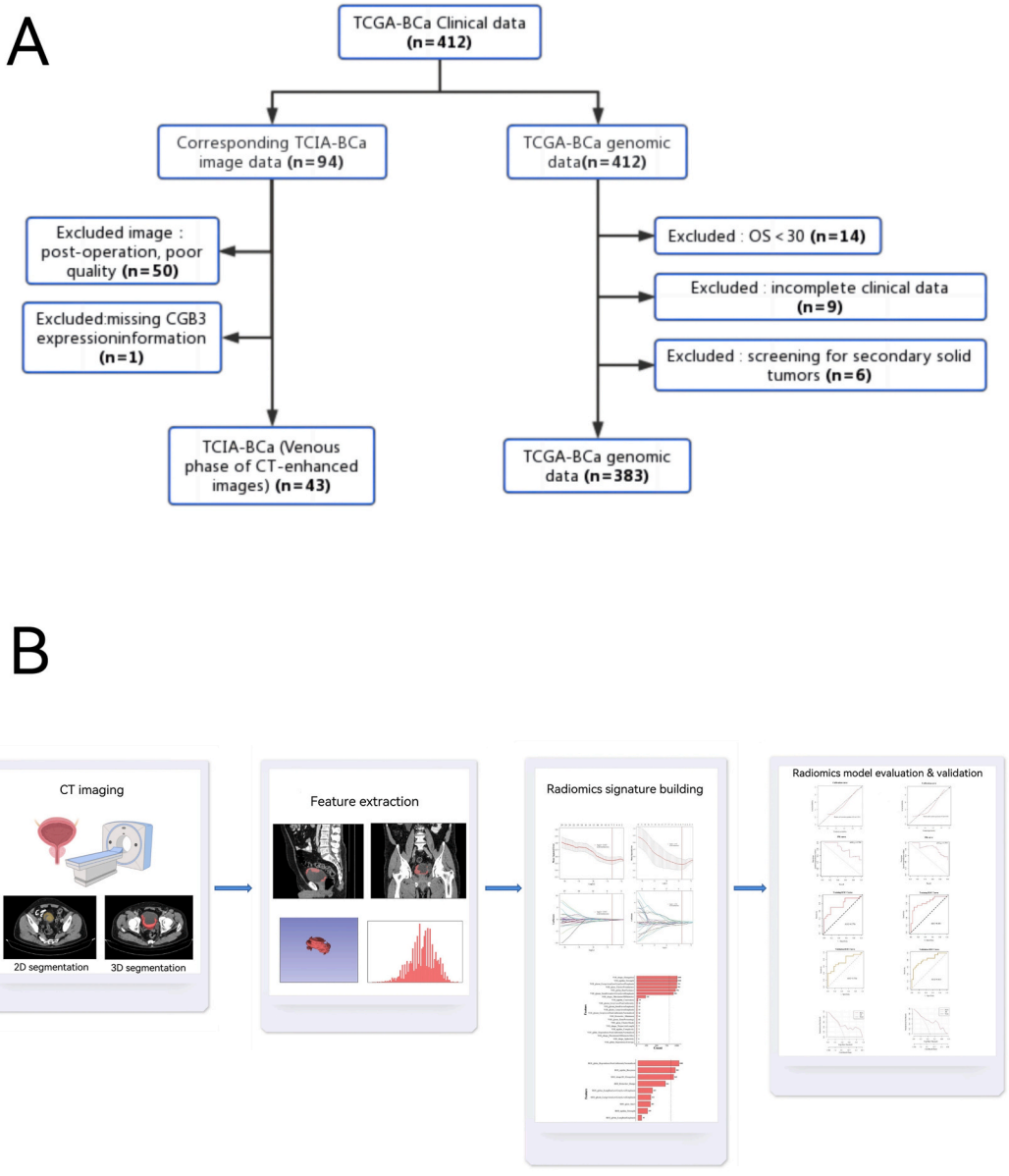

Fig. 1. The brief flowchart of data collection and analysis. (**A**) Gene and image data screening process (Inclusion/exclusion criteria). (**B**) Brief flowchart of radiomic progression.

express multiple β-hCG mRNA isoforms simultaneously are indicative of poorly differentiated tumors and are prone to infiltration [7]. In an ongoing clinical trial (NCT00082706 Phase II trial, chemotherapy for uroepithelial carcinoma), β-hCG is used as a tumor marker for Bca as well as to assess disease progression [8]. A previous study has found that in T2-T4 Bca, elevated urinary β-hCG levels before treatment are a brand of poor prognosis [9]. The beta subunit of hCG is encoded by a set of highly homologous genes (human chorionic gonadotropin beta subunit, CGB, tagged CGB1-CGB9), which also determines its immunological properties [10]. As an affiliate of the glycoprotein hormone chain family, CGB3 (Chorionic Gonadotropin Subunit Beta 3, CGB, HCGB) encodes the β3 subunit of β-hCG (https://www.genecards.org/cgi-bin/carddisp.pl?gene=CGB3). It was found that the CGB gene products are expressed in Bca which may be involved in and drive tumor development [11,12]. Therefore, the accurate estimation of CGB3 expression may accept important implications for the analysis prognosis of tumors.

In the last two decades, the acreage of computer-aided medical image assay has evolved considerably. Many precision radiological imaging technologies are beginning to be applied to the non-invasive and accurate diagnosis and prognostic assessment of tumors [13–18]. The heterogeneity of cancer is closely related to histobiological features such as the proliferation of the abnormal cell, necrosis, angiogenesis and fibrosis [19]. Features that were extracted from medical imaging can reflect potential temporal heterogeneity and spatial heterogeneity of tumors, providing effective information for identifying muscle invasion of tumors, pathological grading, and assessing prognosis [10,20,21]. Radiomics extracts high-throughput image features and acquires massive image parameters to non-invasively and dynamically detect and quantitatively reflect tumor characteristics.

It has been shown that radiomics can be used for early diagnosis and staging of Bca, and can also be applied to tumor recurrence and assessment of response to chemotherapy. Radiomics is also affirmed as a tool for evaluating residual cancer neoplasia and tumor microenvironment (TME) [22–25]. However, many radiomics models are not sufficiently interpretable, the high-throughput characteristics and specific biological features are not clearly defined, and there are some limitations.

Currently, there are few studies applying radiomics accumulated with genes or transcriptome data for the prediction of Bca treatment and prognosis [26–28]. In our study, we extracted the imaging data of Bca as well as the mRNA expression level of CGB3 in Bca through The Cancer Genome Atlas (TCGA) and The Cancer Imaging Archive (TCIA) databases. The radiomics and CGB3 expression were utilized to further predict the prognosis of Bca and provide a basis for clinical treatment planning.

1.1. Retrieval and processing of data

Data from 412 Bca patients in the portal system of TCGA (https://portal.gdc.cancer.gov/) was downloaded and processed. Preoperative CT imaging of 94 Bca patients was collected from TCIA (https://wiki.cancerimagingarchive.net/display/Public), while the transcriptomic message from TCGA was applied for feature extraction in radiomics and modeling. We used the clinical data of 43 patients from the TCGA and TCIA databases for model evaluation in radiomics. Imaging and clinical data were deidentified and authorized by the Institutional Review Board of the TCIA host institution. Exclusion criteria include: incomplete clinical data; missing survival data; without the expression of CGB3; time of survival which is less than 30 days; without CT images; poor quality of CT images without corresponding gene (Fig. 1A).

1.2. Bioinformatics analysis

This study utilized medical imaging and transcriptome data (with clinical and follow-up data) provided by TCGA and TCIA databases. We carried out the characterization of the expression profiles of the genes. RNA seq data was uploaded and transferred in Transcripts Per Kilobase of exon model per Million mapped reads (TPM) format. BLCA (bladder uroepithelial carcinoma) for TCGA and corresponding in GTEx normal tissue data were extracted. Cancerous and non-cancerous tissues were not necessarily from the same patient. Patients with RNA-seq expression were included in the analysis, and those without CGB3 expression were excluded. The survival probabilities and median survival times (MST) were calculated with Kaplan-Meier (KM) curves and log-rank tests. The variables impacting overall survival (OS) were examined in univariate and multivariate analyses using the Cox regression analysis. The interaction between CGB3 and other variables was examined using the likelihood ratio test. Fisher's exact test was used to complete the correlation analysis between the clinical characteristics of cancer and CGB3.

To evaluate immune cell infiltration, transcriptome expression profiles of Bca were transferred to the CIBERSORTx database (https://cibersortx.stanford.edu/), in which every specimen was figured out. For the correlation analysis between CGB3 and immune cell infiltration, Spearman correlation analysis was performed. Gene Ontology (GO) and Kyoto Encyclopedia of Genes and Genomes (KEGG) enrichment analysis of differently expressed genes (DEG) was carried out with the program package of "clusterProfiler" in R software. The correlation analysis of CGB3 with cytokine-related genes was presented by Spearman's rank correlation coefficient.

1.3. Feature extraction of radiomics and model construction

Fig. 1B shows the whole process of image processing.

The device information and scanning parameters of Contrast-enhanced computed tomography (CECT): Manufacturer: GE, SIEMENS; X-ray tube voltage: median 120 kVp; Slice thickness: median 2.5 mm; X-ray tube current: median 210 mA; Pixel spacing: median 0.8×0.8 mm^2.

The entire tumor area was manually outlined to obtain a three-dimensional (3D) whole-tumor area with 3D Slicer software (Version 4.10.2). Based on the whole-tumor region, Python's SimpleITK package (https://simpleitk.org/) was used to automatically obtain the region at the largest level of the tumor. To extract the image features, the "pyradiomics"program package in Python was applied. The

data were normalized based on the two-dimensional (2D) largest tumor level (region of interest, ROI) and three-dimensional (3D) whole-tumor (volume of interest,VOI). Extracted image radiomics features were screened separately using the least absolute shrinkage and selection operator regression (LASSO). A logistic regression method (LR) was applied to fit the radiomics characterization screened by repeated LASSO.

On this basis, the established logistic regression model was subjected to two-way stepwise regression for further feature selection. The subset of characteristics with the smallest Akaike information criterion (AIC) was selected to build the final radiomics model for predicting the levels of CGB3. Radiomics features were derived by two experienced radiology specialists independently based on their manual outlining. The consistency of these features was evaluated with interclass correlation efficiency (ICC). After one physician had completed sketching all cases and outlining the whole tumor area (3D VOI) of each sample, another physician chose 10 samples at random and used the "random number table method" for secondary outlining before features extraction. ICC$\geq$0.75 is often considered as being in high agreement, 0.51–0.75 is moderate, and below 0.50 is considered poor agreement. ICC$\geq$0.75 was taken as the condition for compliance with subsequent analysis.

1.4. Model evaluation and validation

The validity of the radiomics model was evaluated in the training set, while radiomic signatures validation (10-fold cross-validation) was carried out. The Hosmer-Lemeshow goodness-of-fit test was employed to assess the calibration of the CGB3-predicting radiomics mode and to generate a calibration curve. The extent of the clinical benefit of radiomics predictive modeling was demonstrated by plotting decision curves. Intergroup variability in radiomics predictive values was further assessed. The radiomics score (Rad_score) was compared between low levels of CGB3 and high levels of CGB3 molecular subgroups using the Wilcoxon test.

1.5. Statistics and analysis

Statistics and analysis of data were performed with R software (Version 4.1.0). A bilateral $p <$ of 0.05 was accepted as statistically significant. The radiomics model's accuracy (ACC), specificity (SPE), sensitivity (SEN), positive predictive value (PPV) and negative predictive value (NPV) were assessed in the training and validation groups (10-fold cross-validation). In addition, the overall quality of the radiomics model was evaluated with ROC curves, and the performance was comprehensively evaluated by Precision-Recall (PR) curves. The area under the curve (AUC) was computed. To evaluate how well the radiomics prediction model has been calibrated, the Hosmer-Lemeshow goodness-of-fit test was applied. The radiomics evaluation for applications in clinical practice was disclosed with a decision curve analysis (DCA).

2. Results

2.1. CGB3 was discovered to be a DEG

2.1.1. Comparison of clinical characterization of CGB3

The "surf"program package was applied to measure the cutoff of levels of CGB3 (Cutoff = 0.039), while the patients were divided into groups with high and low levels of CGB3.

Table 1
Clinical characteristics of the population with high and low CGB3 expression group.

Variables	Total (n = 383)	Low (n = 192)	High (n = 191)	p
Age, n (%)				0.115
~59	84 (22)	49 (26)	35 (18)	
60~	299 (78)	143 (74)	156 (82)	
Gender, n (%)				0.976
Female	101 (26)	50 (26)	51 (27)	
Male	282 (74)	142 (74)	140 (73)	
Histologic_grade, n (%)				0.031
Low	18 (5)	14 (7)	4 (2)	
High	365 (95)	178 (93)	187 (98)	
Lymphovascular_invasion, n (%)				0.87
NO	121 (32)	59 (31)	62 (32)	
Unknown	125 (33)	65 (34)	60 (31)	
YES	137 (36)	68 (35)	69 (36)	
Pathologic_stage, n (%)				0.185
I/II	123 (32)	70 (36)	53 (28)	
III	134 (35)	62 (32)	72 (38)	
IV	126 (33)	60 (31)	66 (35)	
Histological_subtype, n (%)				0.29
Non-Papillary	260 (68)	125 (65)	135 (71)	
Papillary	123 (32)	67 (35)	56 (29)	

Categorical variables are expressed as percentages, compared with chi-square tests. A two-sided $p < 0.05$ was considered statistically significant.

Table 1 displayed a comparison of the clinical characterization of CGB3. Except for histologic grading in clinical variables, there was no significant difference compared to the high with low levels of CGB3 groups.

2.2. Differences in expression levels of CGB3 in tissues and comparison between survival statistics

As shown in Fig. 2A, there were significantly lower levels of CGB3 in natural tissues than in carcinoma tissues ($P < 0.001$). The MST was 47.43 months in the CGB3 low levels group compared to 27.83 months in the high levels group. High levels of CGB3 were remarkably correlated with a decrease in overall survival, as revealed by Kaplan-Meier curves ($p = 0.029$) (Fig. 2B).

2.3. Association between OS and characteristics of clinicopathology with the Cox regression analysis

High levels of CGB3 were a statistically significant risk variable for OS in univariate analysis (HR = 1.27, 95% confidence interval (CI):1.024–1.574, $p = 0.029$). In addition, high levels of CGB3 were also a statistically significant risk factor for OS in a multifactorial analysis (HR = 1.264, 95% CI:1.018–1.571, $p = 0.034$) (Fig. 2C) .

2.4. Association between CGB3 and immune infiltration enrichment

Spearman's rank correlation heatmap revealed that the levels of CGB3 were positively correlated with plasma cell infiltration ($p < 0.05$). In contrast, CGB3 was correlated with T cell gamma delta infiltration negatively. ($p < 0.05$). It seemed that CGB3 does not significantly correlate with B-cell naive infiltration versus B-cell memory infiltration (Fig. 3A).

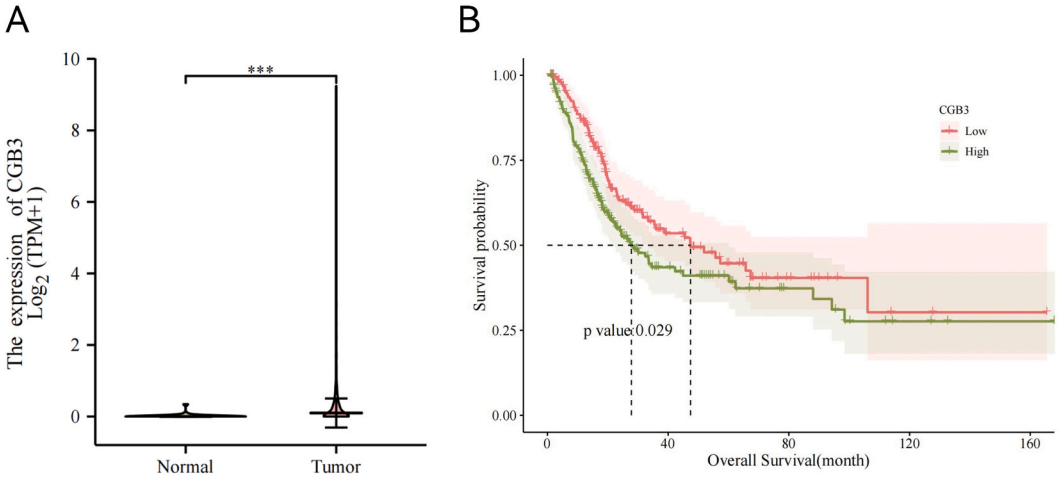

C

Characteristics	Unadj.HR(95%CI)	P value	Adj.HR(95%CI)	P value
CGB3				
High vs. Low	1.27(1.024−1.574)	0.029	1.264(1.018−1.571)	0.034
Age				
60~ vs. ~59	2.01(1.284−3.147)	0.002	1.646(1.045−2.591)	0.032
Gender				
Male vs. Female	0.838(0.602−1.167)	0.296	0.829(0.593−1.16)	0.274
Histologic_grade				
High vs. Low	2.763(0.683−11.176)	0.154	1.141(0.269−4.843)	0.858
Lymphovascular_invasion				
Unknown vs. NO	1.813(1.201−2.738)	0.005	1.751(1.156−2.653)	0.008
YES vs. NO	2.481(1.682−3.658)	< 0.001	1.788(1.172−2.729)	0.007
Pathologic_stage				
III vs. I/II	1.711(1.106−2.647)	0.016	1.616(1.03−2.536)	0.037
IV vs. I/II	3.079(2.044−4.639)	< 0.001	2.419(1.536−3.81)	< 0.001
Histological_subtype				
Papillary vs. Non−Papillary	0.625(0.434−0.901)	0.012	0.809(0.555−1.178)	0.269

Fig. 2. Comparison of the CGB3 expression level between the normal tissues and Bca tissues and the comparison of survival data.(**A**)The expression level of CGB3 in Bca tissues and in normal tissues; (**B**) Kaplan-Meier curves showed that high expression of CGB3 was significantly associated with OS deterioration; (**C**) High CGB3 expression was a statistically significant risk factor for OS in both univariate analysis and multifactorial analysis.

2.5. Relationship with tumor clinical characteristics

Fisher's exact test was developed to carry out the relevance analysis between CGB3 and the clinical features of Bca, which was presented in pie charts. There was a significant association between CGB3 levels and histologic grading ($p = 0.027$); There was no significant correlation with other characteristics such as age, gender, histological subtype, and lymphatic invasion ($p > 0.05$) (Fig. 3B).

2.6. Subgroup analysis and test for interaction

High levels of CGB3 were identified as a risk variable for OS in the subgroup with non-papillary histological subtype in subgroup analysis (HR = 1.106, 95% CI:0.789–1.552), which was not statistically significant. There was a statistically significant difference in elevated CGB3 levels as a danger factor for OS in that particular subgroup with papillary histological subtype (HR = 2.881, 95% CI:1.486–5.587); The interaction test resulted in a p-value of 0.014, which concluded that there was a significant interaction of histological subtype on the association of CGB3 with the OS of patients (Fig. 3C).

2.7. Analysis of GO and KEGG enrichment of CGB3

Enrichment analysis and visualization of the top 10 significantly enriched pathways were performed for biological processes (BP), molecular functions (MF) and cell components (CC), respectively. Enrichment analysis and visualization of 30 significantly enriched pathways were performed for KEGG. GO enrichment analysis showed that DEGs of CGB3 high/low levels groups were enriched in pathways associated with the initiation of DNA replication and ATP-dependent activity acting on DNA, and the results were significant (Fig. 4A). KEGG enrichment analysis showed that DEGs in the CGB3 high/low levels groups were prominently enriched in the cell cycle, chemoattractant-receptor activation, and other signaling pathways (Fig. 4B).

2.8. Relevance analysis of cytokine-related genes

CGB3 was significantly positively correlated ($p < 0.01$) with cytokine-related genes such as CALCR and CRLF1 (*, $p < 0.05$; **, $p < 0.01$; ***, $p < 0.001$) (Fig. 5).

2.9. Radiomics features extraction and modeling

Python was employed to extract the image data, with 102 radiomics features for ROI and 107 radiomics features for VOI.

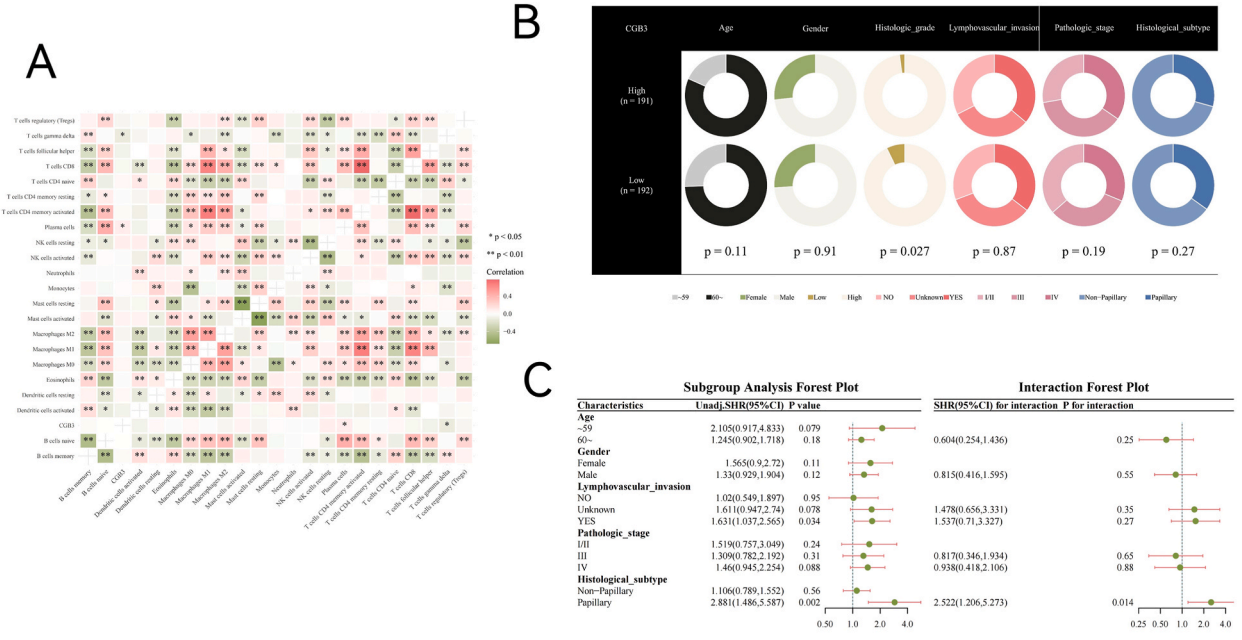

Fig. 3. (**A**) Relationship between CGB3 expression levels and the abundance of immune infiltrates; (**B**) Relationship between CGB3 expression levels and tumor clinical characteristics; (**C**) The interaction test revealed a significant interaction between histological subtype and "association of CGB3 with OS of patients".

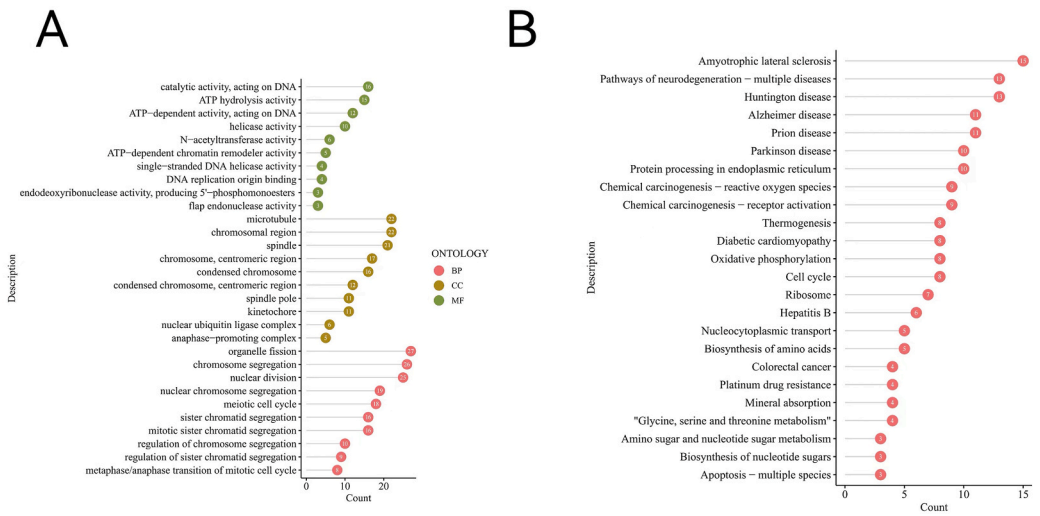

Fig. 4. GO and KEGG enrichment analysis of CGB3. (**A**)The GO enrichment analysis. The horizontal coordinates indicate the number of enriched genes, BP represents biological processes, CC represents cell components and MF represents molecular functions. (**B**) The KEGG enrichment analysis.

2.10. Feature selection and model construction for ROI

1000 LASSO regression features were screened on the 2D_ROI radiomics features of the training set, and the features with frequencies greater than 800 were selected for subsequent model construction. There were 3 filtered features finally selected: ROI_gldm_DependenceNonUniformityNormalized, ROI_ngtdm_Busyness, and ROI_shape2D_Elongation (Fig. 6A and C, Fig. 7A). The weight coefficients indicating the features in the LR algorithm and visualization of prediction results were shown in Fig. 8A and C.

The radiomics formula was constructed by using the Rad_score calculated： radiomics formula = feature * corresponding coefficient (Estimate) + Intercept value (Estimate) (Table 2).

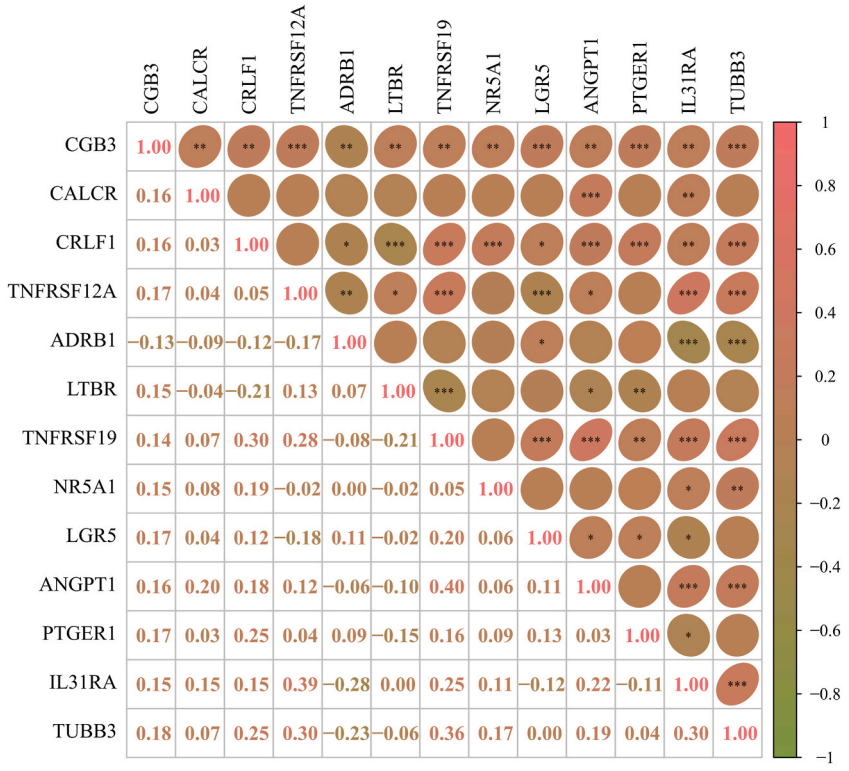

Fig. 5. Relevance analysis of cytokine-related genes.

2.11. Feature screening and model construction for VOI

1000 LASSO regression features were screened on the 3D_VOI radiomics features of the training set. The features with frequencies greater than 800 were selected for inclusion in the subsequent model construction, among which 6 features with frequencies greater than 800 were selected: VOI_ngtdm_Strength, VOI_shape_Elongation, VOI_glcm_ClusterProminence,VOI_glszm_LargeAreaLowGrayLevelEmphasis, VOI_glrlm_RunVariance,VOI_glszm_SmallAreaLowGrayLevelEmphasis (Fig. 6B,D, Fig. 7B). The figure represents the weight coefficients of the filtered features in the LR algorithm and visualization of prediction results were shown in Fig. 8B and D.

The radiomics formula was constructed by using the Rad_score calculated： radiomics formula = feature * corresponding coefficient (Estimate) + Intercept value (Estimate) (Table 3).

Radiomics model evaluation and validation: performance of predicted CGB3 expression levels by 10-fold cross-validation.

The predicted probabilities of the prediction model for the CGB3 high expression levels closely match the realized values in the ROI_LR model (Fig. 9A and B). The AUC of the ROI_LR model was 0.776 in the training and 0.754 in the validation set (Fig. 9C and D). DCA showed high clinical utility of the model (Fig. 9E).

The predicted probabilities of the prediction model for the CGB3 high expression levels closely match the realized values in the VOI_LR model (Fig. 10A and B). The AUC of the ROI_LR model was 0.841 in the training set and 0.815 in the validation set, respectively (Fig. 10C and D). DCA indicated that the model has high clinical utility (Fig. 10E).

The AUCs of the VOI_LR model were superior to those of the ROI_LR model in the training set; the cross-validation AUCs of the VOI_LR model were superior to those of the ROI_LR model. The Delong test revealed that the AUCs of the two models were not statistically different (training set: $p = 0.38$; cross-validation: $p = 0.55$) and both of them had a good predictive performance. The VOI_LR model provided more accuracy than the ROI_LR model.

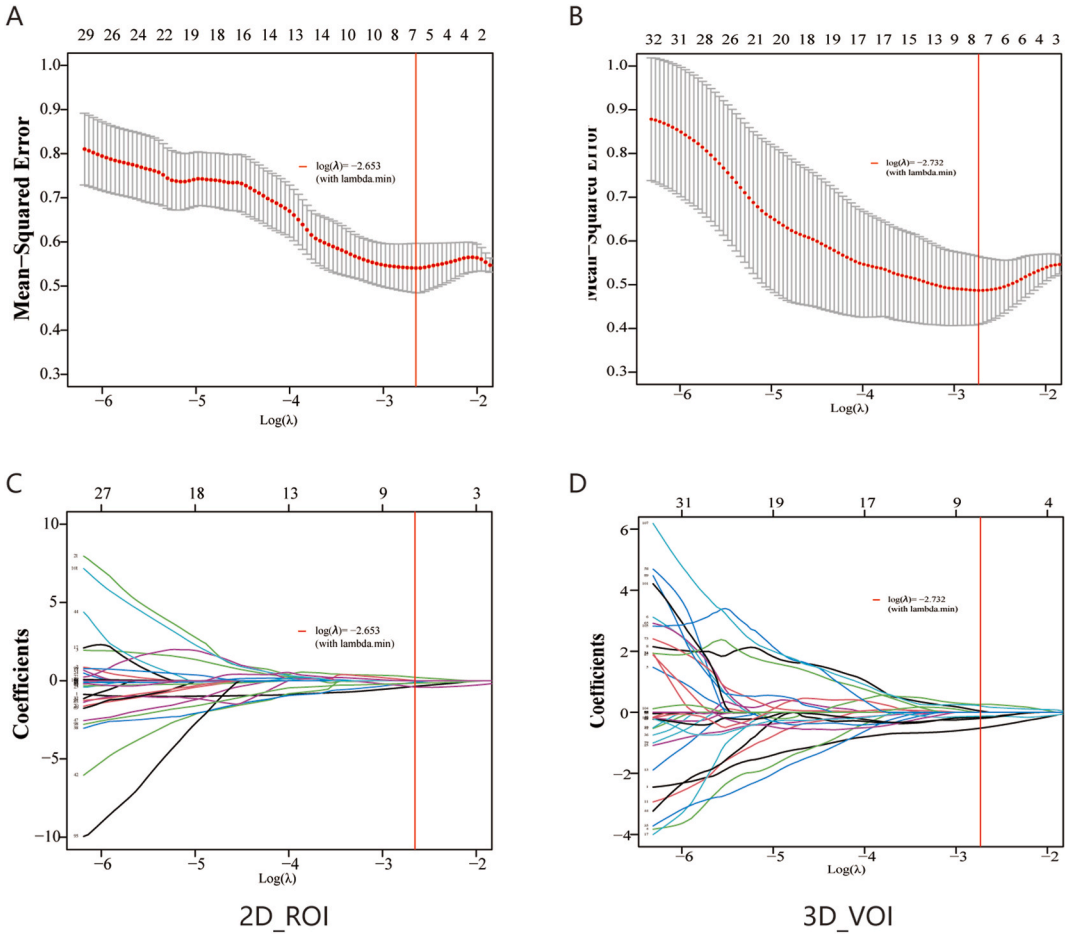

Fig. 6. Feature selection and model construction for ROI and VOI. **(A,B)**Optimal hyperparameter λ values were selected using 10-fold cross-validation in the ROI and VOI LASSO regression models, with the lowest being the feature that best matched the true results. LASSO regression models identified ROI (**C**) and VOI (**D**) radiomics features with nonzero coefficients.

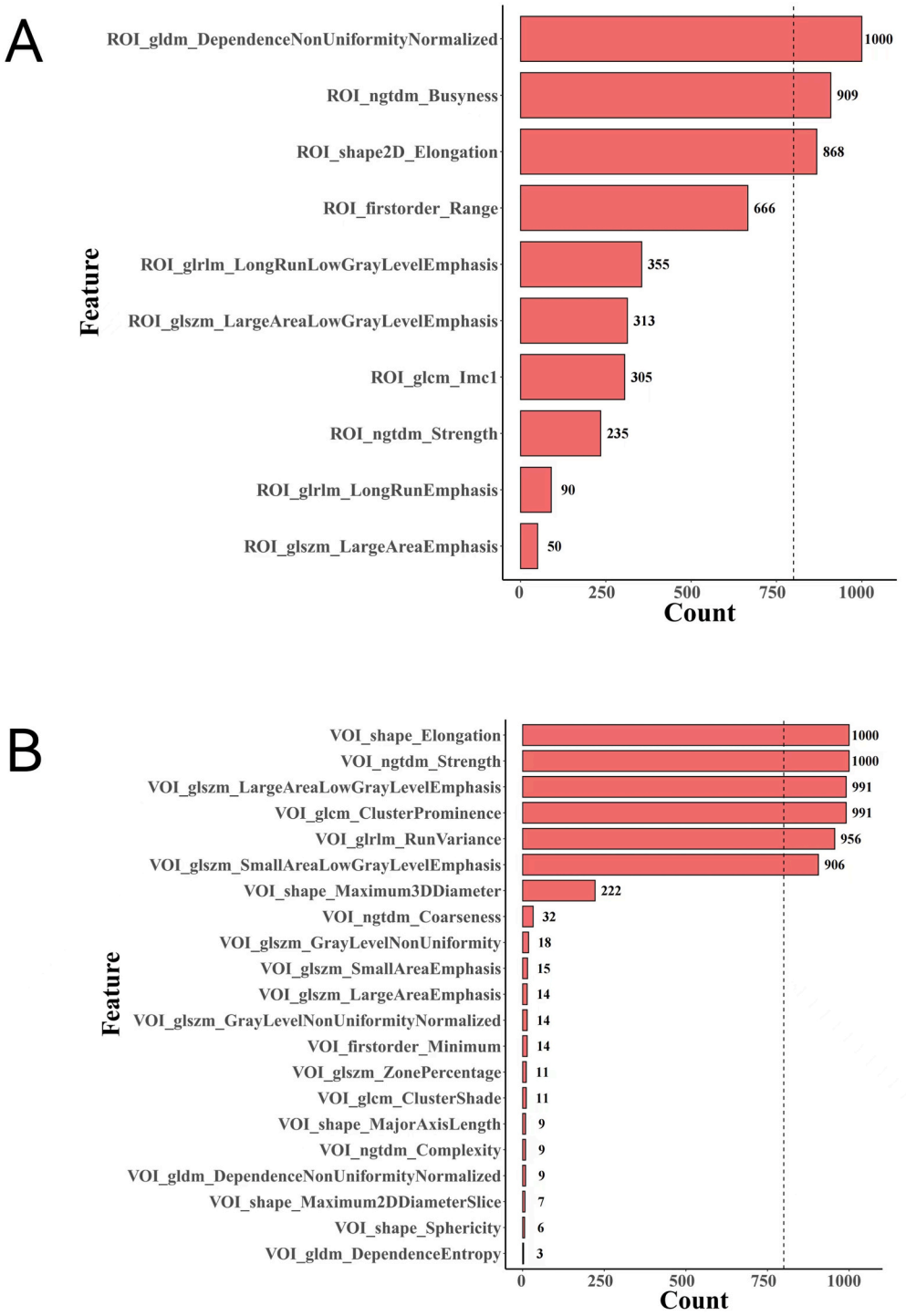

Fig. 7. Histogram of the frequency of features filtered. **(A)**Histogram of the frequency of features filtered by Lasso for ROI; (**B**) Histogram of the frequency of features filtered by Lasso for VOI.

2.12. Comparison of differences in the training set between radiomics scores with the Wilcoxon test

2.12.1. Analysis of variance between ROI_LR model groups

The Rad_score in the low levels of the CGB3 group was significantly lower than that in the high levels of CGB3 group in the training set ($p < 0.01$). ($p \geq 0.05$; *, $p < 0.05$; **, $p < 0.01$; ***, $p < 0.001$; ****,0.0001). (Fig. 9F).

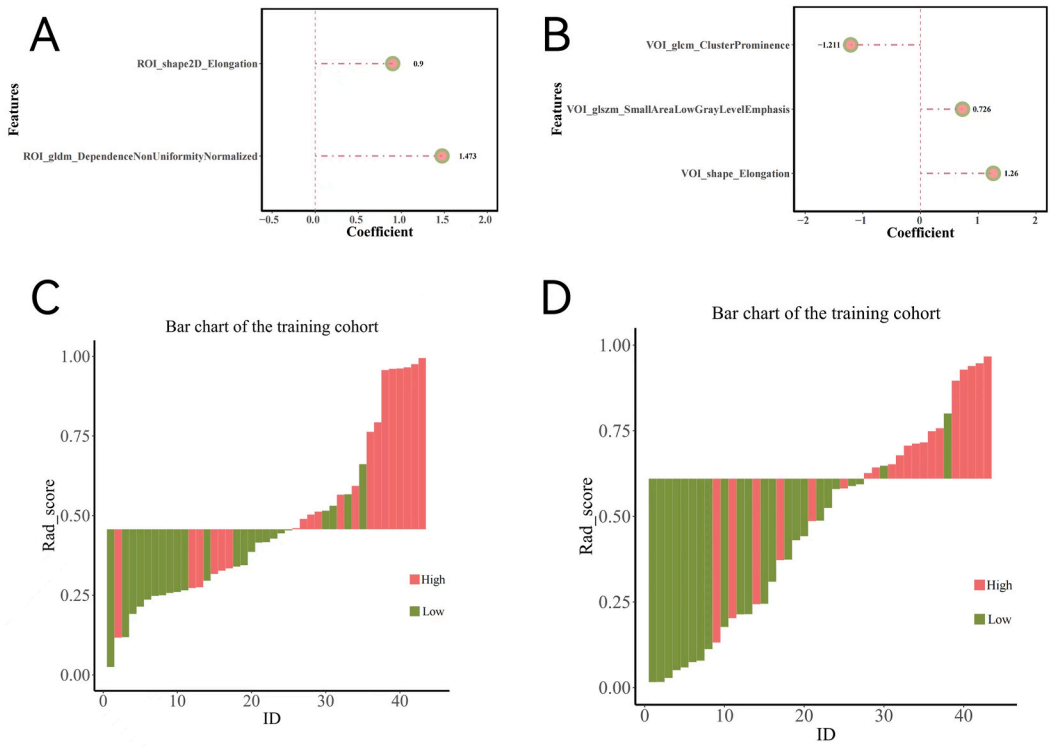

Fig. 8. Weight coefficients of the filtered features in the LR algorithm. (**A**)Weight coefficients of the filtered features in the LR algorithm for ROI; (**B**) Weight coefficients of the filtered features in the LR algorithm for VOI; (**C**)Visualization of prediction results for ROI; (**D**)Visualization of prediction results for VOI.

Table 2
Formula of the ROI radiomics model.

	Estimate	Std. Error	z value	Pr (>|z|)
(Intercept)	0.018273811	0.384447528	0.047532653	0.962088706
ROI_gldm_DependenceNonUniformityNormalized	1.473332472	0.641158371	2.297922852	0.02156618
ROI_shape2D_Elongation	0.900473751	0.452539647	1.989822898	0.046610448

Table 3
Formula of the VOI radiomics model.

	Estimate	Std. Error	z value	Pr (>|z|)
(Intercept)	0.018273811	0.384447528	0.047532653	0.962088706
ROI_gldm_DependenceNonUniformityNormalized	1.473332472	0.641158371	2.297922852	0.02156618
ROI_shape2D_Elongation	0.900473751	0.452539647	1.989822898	0.046610448

2.12.2. Analysis of variance between VOI_LR model groups

It was found that the Rad_score of the high levels of the CGB3 group was dramatically higher in the training set. This was remarkably different from the Rad_score of the low levels of CGB3 group ($p < 0.0001$) ($p \geq 0.05$; *, $p < 0.05$; **, $p < 0.01$; ***, $p < 0.001$; ****,0.0001). (Fig. 10F).

2.13. Consistency evaluation

The median ICC of the VOI radiomics features was 0.884 and there were 87 features with an ICC≥0.75 (Table 4). The median ICC of the ROI radiomics features was 0.892, of which 84 features with ICC≥0.75 (Table 5). All the ICCs of the screened radiomics features were higher than 0.75 (Table 6).

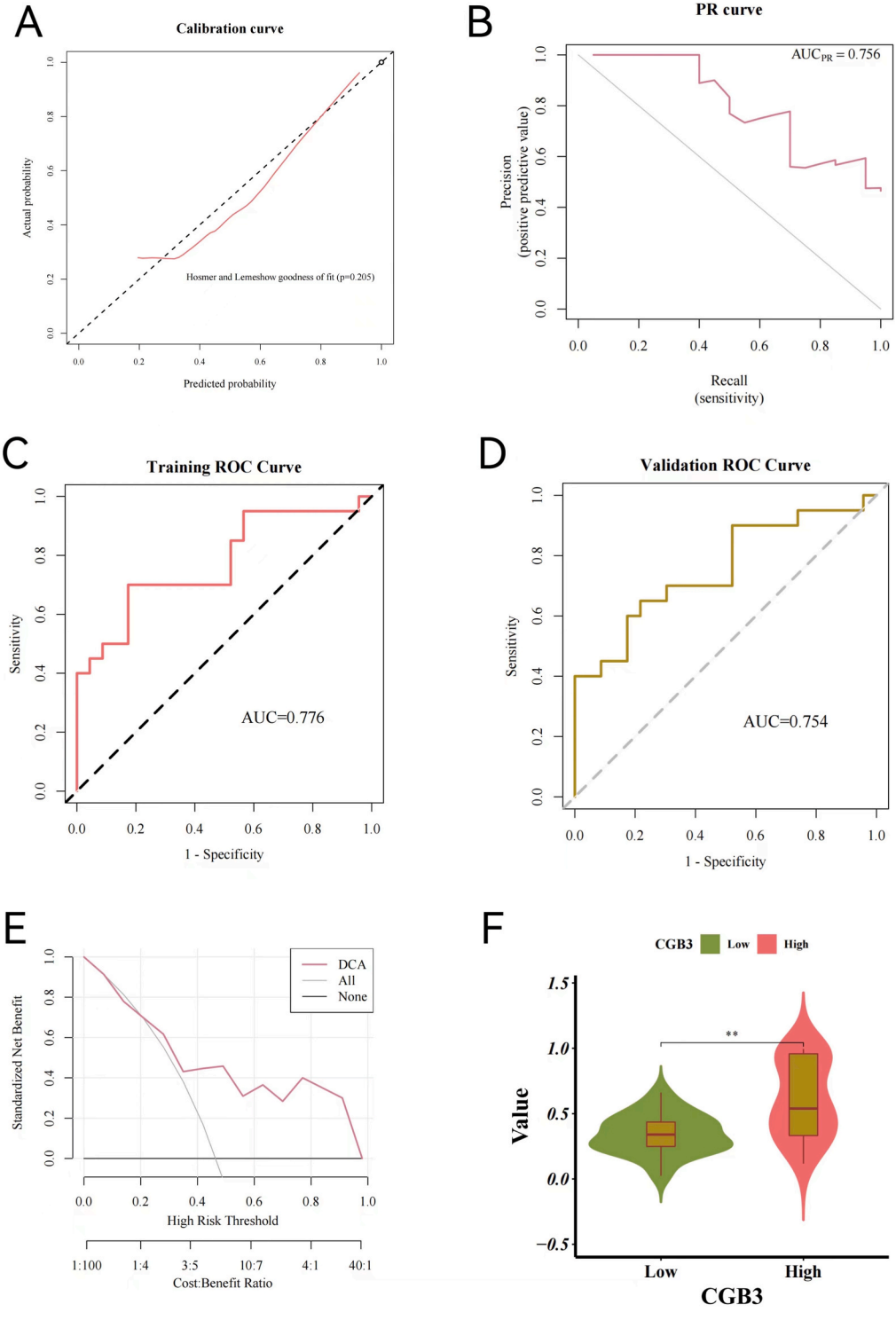

(caption on next page)

Fig. 9. The performance of the ROI radiomics model for predicting the CGB3 expression level with 10-fold cross-validation on the training and validation set. (**A**) Calibration curves of the ROI model. A calibration curve describes the consistency between the predicted and gene expression levels. The 45-degree dotted black line represents the ideal prediction performance; the solid red line represents the model's prediction performance. The closer the solid red line is to the ideal dotted line, the better the model's prediction accuracy. (**B**)Precision- Recall (PR) curve of the ROI model. The X-axis of the recall curve is the actual positive rate (Recall), and the Y-axis is the precision rate. The area under the curve (AUC)-PR is the average accuracy calculated for each coverage threshold. The more convex the turn to the upper right, the better the model's performance. (**C**)A receiver operating characteristic (ROC) curves of the ROI model in the training set. (**D**)ROC curves of the ROI model in the validation set. (**E**) Decision curve analysis (DCA) for the ROI model. The y-axis measures the net beneft. The red curve represents the radiomics model; the gray curve represents the assumption that all patients were treated and the straight black line at the bottom of the figure represents the assumption that no patients were treated. (**F**) Analysis of variance between ROI_LR model groups.

3. Discussion

A research approach combining radiomics and bioinformatics analysis was employed in the study to explore the potential of underlying molecular mechanisms associated with expression levels of CGB3 and develop a CGB3-predicting radiomics model. We predicted the mRNA expression of CGB3 in Bca by CECT radiomics and evaluate the association of the constructed radiomics model with prognosis. We found that both 3D and 2D radiomics models can predict the expression levels of CGB3 and can also be used to assess its prognosis.

According to guideline recommendations [29,30], tumor grading, staging and tumor muscle infiltration status (MIS) are important predictors for the recurrence of bladder cancer, which are important for clinical decision-making and tumor prognosis. Accurate prediction of prognosis is the key to Bca treatment. High expression levels of β-hCG have now been revealed to exist in tumors of multiple tissue-organ origins, while studies have also found that Bca expresses multiple β-hCG isoforms suggesting poor tumor differentiation and poor prognosis [7–9]. CGB3 is the most important subunit encoding β-hCG and may contribute to tumorigenesis and tumor progression. In our study, high expression levels of CGB3 are a risk component for OS in Bca and can be a valid indicator of clinical prognosis of Bca. Based on this, radiomics model construction was performed subsequently. Our findings suggested that a higher Rad_score is associated with higher levels of CGB3, which indirectly indicates a lower survival rate in patients with a high Rad_score. This suggested high levels of CGB3 are associated with poor prognosis in Bca patients. Therefore, it is feasible to use radiological prediction models to predict disease prognosis based on the characteristics of CGB3.

Bioinformatics analysis showed that CGB3 was correlated in a positive way with the infiltration of plasma cells ($p < 0.05$), while in a negative way with the degree of T cell gamma delta infiltration ($p < 0.05$). Plasma cells are thought to be terminally differentiated B cells that generate antibodies against tumors based on tumor-associated antigens [31,35]. Studies of different cancers revealed that elevated infiltration of plasma cells predicted a worse prognosis as well as a poorer response to immunotherapy in individuals [32–34]. It was found that the TLR4 was expressed at low levels in Bca, and low levels of TLR4 were correlated with a high level of plasma cells, which indicated that an increased level of plasma cell infiltration may be a sign of a poor prognosis in Bca [36]. T cell gamma delta is a type of T cell, a lymphocyte with extremely natural immunological properties and an adaptive immune response. T cell gamma delta is capable of producing antibody-dependent cell-mediated cytotoxicity (ADCC) by secreting perforin and granzyme, acting as an antigen-presenting cell for indirect tumor killing [37,38]. Low levels of T cell gamma delta are associated with high levels of CGB3, suggesting that a decrease in T cell gamma delta may be associated with tumor development and progression.

The combination of radiomics with genomics or transcriptomics has already been reported in recent years [39]. Radiogenomics is mainly used to study the relationship between medical images and oncogenes. As a non-invasive test, radiogenomics can comprehensively analyze tumor texture characteristics and genetic heterogeneity within tumors [40–42]. ZT Zheng [42] reported that CD8A is a new marker of prognosis and response to immunotherapy in Bca. The CD8A expression can be predicted preoperatively on the basis of MRI radiomics features in Bca patients. Sheng Wan [43] reported developing radiomics models that could predict CCR5 expression levels to provide a further prognosis for patients with ovarian cancer. The expression levels of CD44 and CD133 in gliomas can be predicted by radiomics features [44]. The above studies further illustrate the potential of radiomics in predicting gene expression in cancers. Furthermore, several studies have revealed a remarkable association between radiomics features based on CT and OS of Bca Patients. Xin Tang [45] studied that the prediction model based on pelvic CECT radiological features had a good ability to predict tumor mutation burden (TMB). Qing Li [46] found that the expression of HRG (histidine-rich glycoprotein) has a significant impact on the prognosis of Bca patients, while radiomics features based on CT can successfully predict the preoperative HRG. These outcomes match those from our analysis. This consistency indicates that CT radiomics have a high ability to predict Bca. In this study, an association between radiological modeling and the prognosis was constructed using 3D_VOL and 2D_ROI CECT combined with the CGB3 gene. The AUCs of the ROI model in the training set and the validation set were 0.776 and 0.754, respectively; The AUCs of the VOI model in the training set and the validation set were 0.841 and 0.815, respectively. Both models had good predictive efficacy and high clinical usefulness.

Both 3D and 2D CT radiomics features had good predictive power for CGB3 in Bca in our results. Radiomics based on the 2D tumor maximum level were found to have predictive value, with applications in prostate cancer [47] and lung cancer [48]. One study found that models established with 2D radiomics characteristics performed similarly to those constructed with three-dimensional features in characterizing gastric cancer [49]. YL Feng [50] reported the prediction of survival of patients with non-small cell lung cancer using 2D and 3D radiomics features. The combination of 2D and 3D showed better prediction performance than radiomics features generated with either 2D or 3D features alone. Our study demonstrated that radiomics based on both 2D and 3D CECT can make an effective prediction of the expression level of CGB3 [50]. The AUCs of the 3D VOI_LR model were superior to that of the 2D ROI_LR model in the

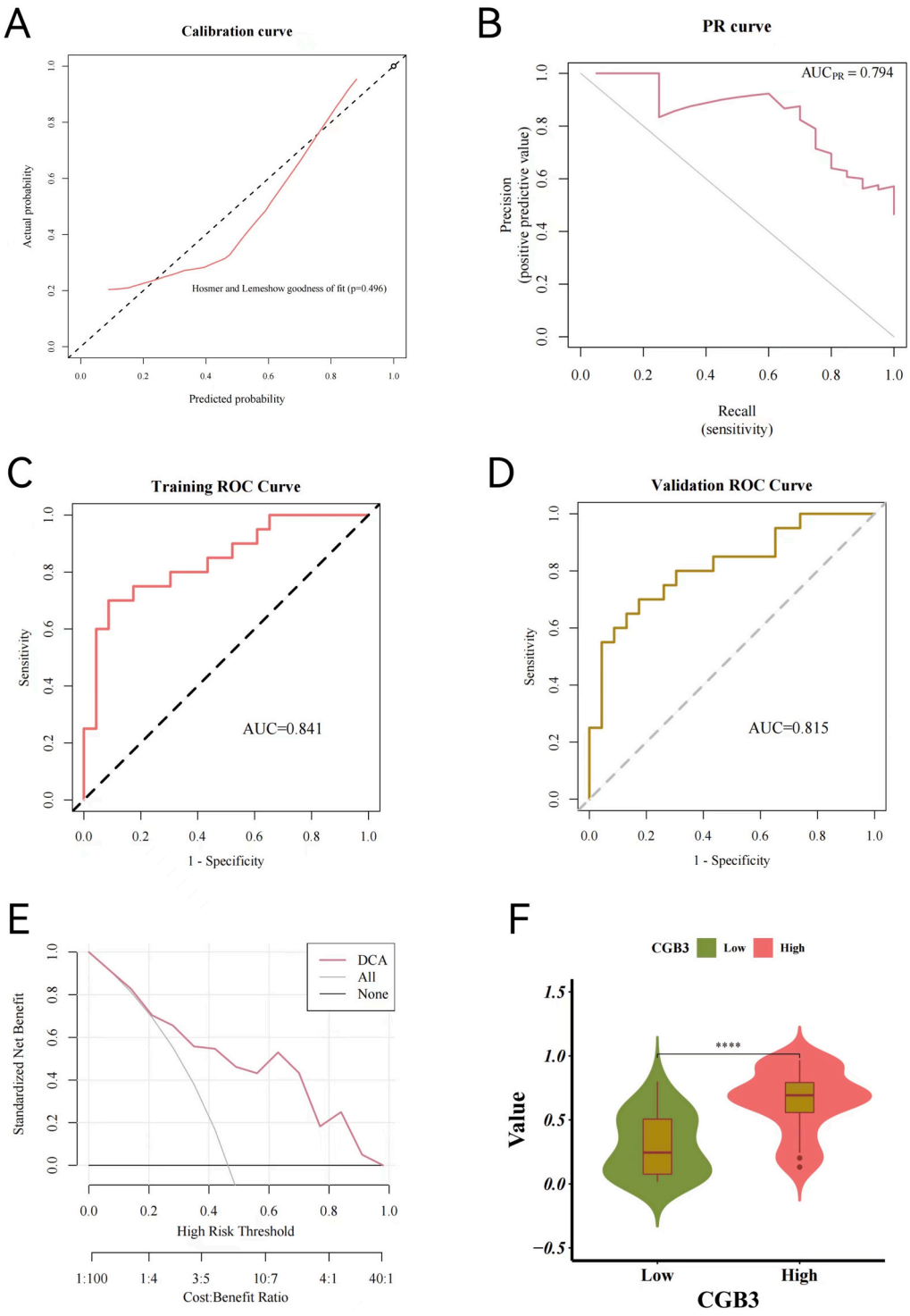

Fig. 10. The performance of the VOI radiomics model for predicting the CGB3 expression level with 10-fold cross-validation on the training and validation set. (**A**)Calibration curves of the VOI model. (**B**)PR curve of the VOI model. (**C**) ROC curves of the VOI model in the training set. (**D**)ROC curves of the VOI model in the validation set. (**E**)DCA for the VOI model. (**F**)Analysis of variance between VOI_LR model groups.

training set, and the precision of the VOI_LR model was higher than that of the ROI_LR model. The performance of 3D radiomics features was observed to be superior in our tests. ICCs screened for radiomics characteristics were higher than 0.75 in both 3D and 2D radiomics models, which reflect a good correlation and agreement between the measurements.

Table 4
The ICC of VOI radiomics features.

	ICC≥0.75	0.5 ≤ ICC<0.75	ICC<0.5	ICC_Mean	ICC_Median
Percentage	0.824	0.157	0.02	0.892	0.954
Number	84	16	2	NA	NA

Table 5
The ICC of ROI radiomics features.

	ICC≥0.75	0.5 ≤ ICC<0.75	ICC<0.5	ICC_Mean	ICC_Median
Percentage	0.813	0.178	0.009	0.884	0.94
Number	87	19	1	NA	NA

Table 6
The ICCs of the screened radiomic features.

	x
VOI_shape_Elongation	0.751991988
VOI_glcm_ClusterProminence	0.980633726
VOI_glszm_SmallAreaLowGrayLevelEmphasis	0.916521272
ROI_gldm_DependenceNonUniformityNormalized	0.950824721
ROI_shape2D_Elongation	0.874559611

There are some limitations to our study. First, because all the image information comes from public databases, we are inevitably subject to image and quality variations. These factors may affect the results of the predictive analysis. Second, this study was retrospective and its generalization remained to be studied. Third, there may have been a certain degree of selection bias in this study. However, the study individuals were a population for which both transcriptomic and radiomics data were available, and the selection bias resulting from the development of inclusion and exclusion criteria to ensure that the results applied to the majority of the population were not significant for this study. Fourth, because of the small sample size, the Cox proportional-hazards model was not applicable to this study. This led to the inability to further predict the prognosis of Bca by radiomics instead of gene expression. Fifth, although the ROIs and VOIs outlined in the images were hand-drawn and supervised by two experienced radiology specialists, it was subjective in nature. Automatic or semi-automatic methods were recommended in further studies to reduce operator interaction during segmentation.

4. Conclusion

Accurate cancer subtype identification and indicators of tumor immune biology are becoming increasingly essential in prognosis and therapy selection. Our study demonstrated that the expression levels of CGB3 can significantly influence the outcomes of patients with Bca. In this study, noninvasive models were developed from CECT radiomics which could efficiently and accurately predict the CGB3 expression. CGB3 can be used as a target in current clinical trials and as an important reference for clinical diagnostic and therapeutic decisions, which facilitates the screening of the superior population corresponding to the target.

Ethics declarations

All of the patient data were obtained from public datasets: the open-access TCGA and TCIA initiatives. Imaging and clinical data have been de-identified by TCIA and approved by the Institutional Review Board of the TCIA hosting institution. All the samples from TCIA and TCGA were anonymized and publicly available and no permission from the local ethics committee was necessary.

Funding statement

This research was supported by the National Natural Science Foundation of China (Grant No.82372685); Medical Science and Technology Research Fund Project of Guangdong Province of China (Grant No.B2023489); Medical Science and Technology Program of Shantou of China (Grant No. [2021]3-11).

Author contribution statement

1 - Conceived and designed the experiments.
2 - Performed the experiments.
3 - Analyzed and interpreted the data.
4 - Contributed reagents, materials, analysis tools or data.
5 - Wrote the paper.

Data availability statement

Data included in article/supplementary material/referenced in article.

Availability of data and materials

The data are publicly available through TCIA website:
https://www.cancerimagingarchive.net/access-data/

Declaration of competing interest

The authors declare that they have no known competing financial interests or personal relationships that could have appeared to influence the work reported in this paper.

Acknowledgements

Not applicable.

Abbreviations

2D	two-dimensional
3D	three-dimensional
AUC	area under the receiver operating characteristic
AIC	Akaike information criterion
Bca	bladder cancer
CECT	contrast-enhanced computed tomography
CT	computed tomography
CI	confidence interval
DCA	decision curve analysis
DEG	differentially expressed genes
GO	Gene Ontology
ICC	intraclass correlation efficiency
KEGG:	Kyoto Encyclopedia of Genes and Genomes
KM	Kaplan-Meier curve
LASSO	the least absolute shrinkage and selection operator regression
LR	logistic regression algorithm
MST	median survival times
OS	overall survival
PR	precision recall curves
Rad_score	radiomics score
ROC:	receiver operating characteristic
ROI	region of interest
TCGA	The Cancer Genome Atlas
TCIA	Cancer Imaging Archive
VOI	volume of interest
TME	tumor microenvironment

References

[1] H. Sung, J. Ferlay, R.L. Siegel, M. Laversanne, I. Soerjomataram, A. Jemal, F. Bray, Global cancer statistics 2020: GLOBOCAN estimates of incidence and mortality worldwide for 36 cancers in 185 countries, CA A Cancer J. Clin. 71 (3) (2021 May) 209–249.
[2] R.L. Siegel, K.D. Miller, N.S. Wagle, A. Jemal, Cancer statistics, 2023, CA A Cancer J. Clin. 73 (1) (2023 Jan) 17–48.
[3] P. Woźnicki, F.C. Laqua, K. Messmer, W.G. Kunz, C. Stief, D. Nörenberg, A. Schreier, J. Wójcik, J. Ruebenthaler, M. Ingrisch, J. Ricke, A. Buchner, G.B. Schulz, E. Gresser, Radiomics for the prediction of overall survival in patients with bladder cancer prior to radical cystectomy, Cancers 14 (18) (2022 Sep 13) 4449.
[4] H.X. Bai, A.M. Lee, L. Yang, P. Zhang, C. Davatzikos, J.M. Maris, S.J. Diskin, Imaging genomics in cancer research: limitations and promises, Br. J. Radiol. 89 (1061) (2016), 20151030.
[5] R.K. Iles, P.J. Delves, S.A. Butler, Does hCG or hCGβ play a role in cancer cell biology? Mol. Cell. Endocrinol. 329 (1–2) (2010 Nov 25) 62–70.
[6] K. Hotakainen, S. Lintula, R. Jarvinen, A. Paju, J. Stenman, E. Rintala, U.H. Stenman, Overexpression of human chorionic gonadotropin beta genes 3, 5 and 8 in tumor tissue and urinary cells of bladder cancer patients, Tumour Biol. 28 (1) (2007) 52–56.
[7] Yongguang Jiang, Puqing Zeng, Chuanguo Xiao, Expression of human chorionic gonadotropin β genes in the tissues of bladder cancer, Chin. J. Urol. 23 (7) (2002) 432–433, 23.

[8] Leucovorin Fluorouracil, Gemcitabine, and cisplatin in treating patients with metastatic or unresectable adenocarcinoma of the urothelium or urachal remnant, Available at: https://clinicaltrials. gov/ct2/show/NCT00082706.

[9] R.K. Iles, R. Persad, M. Trivedi, K.B. Sharma, A. Dickinson, P. Smith, T. Chard, Urinary concentration of human chorionic gonadotrophin and its fragments as a prognostic marker in bladder cancer, Br. J. Urol. 77 (1) (1996 Jan) 61–69.

[10] K. Biskup, V. Blanchard, P. Castillo-Binder, H. Alexander, K. Engeland, S. Schug, N- and O-glycosylation patterns and functional testing of CGB7 versus CGB3/5/8 variants of the human chorionic gonadotropin (hCG) beta subunit, Glycoconj. J. 37 (5) (2020 Oct) 599–610.

[11] P. Białas, A. Śliwa, A. Szczerba, A. Jankowska, The study of the expression of CGB1 and CGB2 in human cancer tissues, Genes 11 (9) (2020 Sep 17) 1082.

[12] Palak Singh, Nakarin Kitkumthorn, Pattamawadee Yanatatsaneejit, Identification of malignancy in PAP smear samples using the CGB3 and NOP56 genes as methylation markers, Asian Pac. J. Cancer Prev. APJCP 23 (10) (2022 Oct 1) 3541–3551.

[13] X. Xu, Y. Liu, X. Zhang, Q. Tian, Y. Wu, G. Zhang, J. Meng, Z. Yang, H. Lu, Preoperative prediction of muscular invasiveness of bladder cancer with radiomic features on conventional MRI and its high-order derivative maps, Abdom Radiol. (NY) 42 (7) (2017 Jul) 1896–1905.

[14] H.C. Thoeny, M.F. Bellin, E.M. Comperat, G.N. Thalmann, Vesical imaging-reporting and data system (VI-RADS): added value for management of bladder cancer patients? Eur. Urol. 74 (3) (2018 Sep) 307–308.

[15] R. Renard-Penna, L. Rocher, C. Roy, M. André, M.F. Bellin, I. Boulay, D. Eiss, N. Girouin, N. Grenier, O. Hélénon, J.F. Lapray, A. Lefèvre, X. Matillon, J. M. Ménager, I. Millet, S. Ronze, T. Sanzalone, J. Tourniaire, S. Brunelle, O. Rouvière, "French society of genitourinary imaging consensus group". Imaging protocols for CT urography: results of a consensus conference from the French society of genitourinary imaging, Eur. Radiol. 30 (3) (2020 Mar) 1387–1396.

[16] H. Li, Y. Zhu, E.S. Burnside, E. Huang, K. Drukker, K.A. Hoadley, C. Fan, S.D. Conzen, M. Zuley, J.M. Net, E. Sutton, G.J. Whitman, E. Morris, C.M. Perou, Y. Ji, M.L. Giger, Quantitative MRI radiomics in the prediction of molecular classifications of breast cancer subtypes in the TCGA/TCIA data set, NPJ Breast Cancer 2 (2016), 16012.

[17] G. Wang, Y. Sun, S. Jiang, G. Wu, W. Liao, Y. Chen, Z. Lin, Z. Liu, S. Zhuo, Machine learning-based rapid diagnosis of human borderline ovarian cancer on second-harmonic generation images, Biomed. Opt Express 12 (9) (2021 Aug 16) 5658–5669.

[18] W.L. Bi, A. Hosny, M.B. Schabath, M.L. Giger, N.J. Birkbak, A. Mehrtash, T. Allison, O. Arnaout, C. Abbosh, I.F. Dunn, R.H. Mak, R.M. Tamimi, C.M. Tempany, C. Swanton, U. Hoffmann, L.H. Schwartz, R.J. Gillies, R.Y. Huang, H.J.W.L. Aerts, Artificial intelligence in cancer imaging: clinical challenges and applications, CA A Cancer J. Clin. 69 (2) (2019 Mar) 127–157.

[19] Rui Zhong, Li Hui, Shuan Zhang, et al., How to recognize and manage tumor heterogeneity? Chin. J. Lung Cancer 21 (9) (2018) 712–718.

[20] Y. Ueno, M. Takeuchi, T. Tamada, K. Sofue, S. Takahashi, Y. Kamishima, N. Hinata, K. Harada, M. Fujisawa, T. Murakami, Diagnostic accuracy and interobserver agreement for the vesical imaging-reporting and data system for muscle-invasive bladder cancer: a multireader validation study, Eur. Urol. 76 (1) (2019 Jul) 54–56.

[21] H. Peng, D. Dong, M.J. Fang, L. Li, L.L. Tang, L. Chen, W.F. Li, Y.P. Mao, W. Fan, L.Z. Liu, L. Tian, A.H. Lin, Y. Sun, J. Tian, J. Ma, Prognostic value of deep learning PET/CT-Based radiomics: potential role for future individual induction chemotherapy in advanced nasopharyngeal carcinoma, Clin. Cancer Res. 25 (14) (2019 Jul 15) 4271–4279.

[22] S. Wu, J. Zheng, Y. Li, H. Yu, S. Shi, W. Xie, H. Liu, Y. Su, J. Huang, T. Lin, A radiomics nomogram for the preoperative prediction of lymph node metastasis in bladder cancer, Clin. Cancer Res. 23 (22) (2017 Nov 15) 6904–6911.

[23] G. Zhang, L. Xu, L. Zhao, L. Mao, X. Li, Z. Jin, H. Sun, CT-based radiomics to predict the pathological grade of bladder cancer, Eur. Radiol. 30 (12) (2020 Dec) 6749–6756.

[24] G.M. Zhang, H. Sun, B. Shi, Z.Y. Jin, H.D. Xue, Quantitative CT texture analysis for evaluating histologic grade of urothelial carcinoma, Abdom Radiol. (NY) 42 (2) (2017 Feb) 561–568.

[25] S.S. Garapati, L. Hadjiiski, K.H. Cha, H.P. Chan, E.M. Caoili, R.H. Cohan, A. Weizer, A. Alva, C. Paramagul, J. Wei, C. Zhou, Urinary bladder cancer staging in CT urography using machine learning, Med. Phys. 44 (11) (2017 Nov) 5814–5823.

[26] A. Dovrou, E. Bei, S. Sfakianakis, K. Marias, N. Papanikolaou, M. Zervakis, Synergies of radiomics and transcriptomics in lung cancer diagnosis: a pilot study, Diagnostics 13 (4) (2023 Feb 15) 738.

[27] Z. Zheng, Y. Guo, X. Huang, J. Liu, R. Wang, X. Qiu, S. Liu, CD8A as a prognostic and immunotherapy predictive biomarker can Be evaluated by MRI radiomics features in bladder cancer, Cancers 14 (19) (2022 Oct 5) 4866.

[28] F. Ye, Y. Hu, J. Gao, Y. Liang, Y. Liu, Y. Ou, Z. Cheng, H. Jiang, Radiogenomics map reveals the landscape of m6A methylation modification pattern in bladder cancer, Front. Immunol. 12 (2021 Oct 18), 722642.

[29] M. Babjuk, M. Burger, O. Capoun, D. Cohen, E.M. Compérat, J.L. Dominguez Escrig, P. Gontero, F. Liedberg, A. Masson-Lecomte, A.H. Mostafid, J. Palou, B.W. G. van Rhijn, M. Rouprêt, S.F. Shariat, T. Seisen, V. Soukup, R.J. Sylvester, European association of urology guidelines on non-muscle-invasive bladder cancer (Ta, T1, and carcinoma in situ), Eur. Urol. 81 (1) (2022 Jan) 75–94.

[30] J.A. Witjes, H.M. Bruins, R. Cathomas, E.M. Compérat, N.C. Cowan, G. Gakis, V. Hernández, E. Linares Espinós, A. Lorch, Y. Neuzillet, M. Rouanne, G. N. Thalmann, E. Veskimäe, M.J. Ribal, A.G. van der Heijden, European association of urology guidelines on muscle-invasive and metastatic bladder cancer: summary of the 2020 guidelines, Eur. Urol. 79 (1) (2021 Jan) 82–104.

[31] G.V. Sharonov, E.O. Serebrovskaya, D.V. Yuzhakova, O.V. Britanova, D.M. Chudakov, B cells, plasma cells and antibody repertoires in the tumour microenvironment, Nat. Rev. Immunol. 20 (5) (2020 May) 294–307.

[32] Z.M. Mohammed, J.J. Going, J. Edwards, B. Elsberger, D.C. McMillan, The relationship between lymphocyte subsets and clinico-pathological determinants of survival in patients with primary operable invasive ductal breast cancer, Br. J. Cancer 109 (6) (2013 Sep 17) 1676–1684.

[33] F.M. Bosisio, J.S. Wilmott, N. Volders, M. Mercier, J. Wouters, M. Stas, W.A. Blokx, D. Massi, J.F. Thompson, R.A. Scolyer, N. van Baren, J.J. van den Oord, Plasma cells in primary melanoma. Prognostic significance and possible role of IgA, Mod. Pathol. 29 (4) (2016 Apr) 347–358.

[34] S. Lundgren, J. Berntsson, B. Nodin, P. Micke, K. Jirström, Prognostic impact of tumour-associated B cells and plasma cells in epithelial ovarian cancer, J. Ovarian Res. 9 (2016 Apr 6) 21.

[35] N.S. Patil, B.Y. Nabet, S. Müller, H. Koeppen, W. Zou, J. Giltnane, A. Au-Yeung, S. Srivats, J.H. Cheng, C. Takahashi, P.E. de Almeida, A.S. Chitre, J.L. Grogan, L. Rangell, S. Jayakar, M. Peterson, A.W. Hsia, W.E. O'Gorman, M. Ballinger, R. Banchereau, D.S. Shames, Intratumoral plasma cells predict outcomes to PD-L1 blockade in non-small cell lung cancer, Cancer Cell 40 (3) (2022 Mar 14) 289–300.

[36] J.L. Lu, Q.D. Xia, Y. Sun, Y. Xun, H.L. Hu, C.Q. Liu, J.X. Sun, J.Z. Xu, J. Hu, S.G. Wang, Toll-like receptor 4 as a favorable prognostic marker in bladder cancer: a multi-omics analysis, Front. Cell Dev. Biol. 9 (2021 Jun 1), 651560.

[37] N. Ji, N. Mukherjee, Z.J. Shu, R.M. Reyes, J.J. Meeks, D.J. McConkey, J.A. Gelfond, T.J. Curiel, R.S. Svatek, Γδ T cells support antigen-specific αβ T cell-mediated antitumor responses during BCG treatment for bladder cancer, Cancer Immunol. Res. 9 (12) (2021 Dec) 1491–1503.

[38] S. Nguyen, M.F. Chevalier, S. Benmerzoug, V. Cesson, A.K. Schneider, S.C. Rodrigues-Dias, F. Dartiguenave, I. Lucca, P. Jichlinski, B. Roth, D. Nardelli-Haefliger, L. Derré, Vδ2 T cells are associated with favorable clinical outcomes in patients with bladder cancer and their tumor reactivity can be boosted by BCG and zoledronate treatments, J. Immunother Cancer 10 (8) (2022 Aug), e004880.

[39] P. Lin, D.Y. Wen, L. Chen, X. Li, S.H. Li, H.B. Yan, R.Q. He, G. Chen, Y. He, H. Yang, A radiogenomics signature for predicting the clinical outcome of bladder urothelial carcinoma, Eur. Radiol. 30 (1) (2020 Jan) 547–557.

[40] R. Jain, L.M. Poisson, D. Gutman, L. Scarpace, S.N. Hwang, C.A. Holder, M. Wintermark, A. Rao, R.R. Colen, J. Kirby, J. Freymann, C.C. Jaffe, T. Mikkelsen, A. Flanders, Outcome prediction in patients with glioblastoma by using imaging, clinical, and genomic biomarkers: focus on the nonenhancing component of the tumor, Radiology 272 (2) (2014 Aug) 484–493.

[41] H. Arita, M. Kinoshita, A. Kawaguchi, M. Takahashi, Y. Narita, Y. Terakawa, N. Tsuyuguchi, Y. Okita, M. Nonaka, S. Moriuchi, M. Takagaki, Y. Fujimoto, J. Fukai, S. Izumoto, K. Ishibashi, Y. Nakajima, T. Shofuda, D. Kanematsu, E. Yoshioka, Y. Kodama, M. Mano, K. Mori, K. Ichimura, Y. Kanemura, Lesion location implemented magnetic resonance imaging radiomics for predicting IDH and TERT promoter mutations in grade II/III gliomas, Sci. Rep. 8 (1) (2018 Aug 6), 11773.

[42] Z. Zheng, Y. Guo, X. Huang, J. Liu, R. Wang, X. Qiu, S. Liu, CD8A as a prognostic and immunotherapy predictive biomarker can Be evaluated by MRI radiomics features in bladder cancer, Cancers 14 (19) (2022 Oct 5) 4866.
[43] S. Wan, T. Zhou, R. Che, Y. Li, J. Peng, Y. Wu, S. Gu, J. Cheng, X. Hua, CT-based machine learning radiomics predicts CCR5 expression level and survival in ovarian cancer, J. Ovarian Res. 16 (1) (2023 Jan 3) 1.
[44] Z. Wang, X. Tang, J. Wu, Z. Zhang, K. He, D. Wu, S. Chen, X. Xiao, Radiomics features based on T2-weighted fluid-attenuated inversion recovery MRI predict the expression levels of CD44 and CD133 in lower grade gliomas, Future Oncol. 18 (7) (2022 Mar) 807–819.
[45] X. Tang, W.L. Qian, W.F. Yan, T. Pang, Y.L. Gong, Z.G. Yang, Radiomic assessment as a method for predicting tumor mutation burden (TMB) of bladder cancer patients: a feasibility study, BMC Cancer 21 (1) (2021 Jul 16) 823.
[46] Q. Li, Y. Luo, D. Liu, B. Li, Y. Liu, T. Wang, Construction and prognostic value of enhanced CT image omics model for noninvasive prediction of HRG in bladder cancer based on logistic regression and support vector machine algorithm, Front. Oncol. 12 (2023 Jan 16), 966506.
[47] S. Monti, V. Brancato, G. Di Costanzo, L. Basso, M. Puglia, A. Ragozzino, M. Salvatore, C. Cavaliere, Multiparametric MRI for prostate cancer detection: new insights into the combined use of a radiomic approach with advanced acquisition protocol, Cancers 12 (2) (2020 Feb 7) 390.
[48] C. Shen, Z. Liu, M. Guan, J. Song, Y. Lian, S. Wang, Z. Tang, D. Dong, L. Kong, M. Wang, D. Shi, J. Tian, 2D and 3D CT radiomics features prognostic performance comparison in non-small cell lung cancer, Transl. Oncol. 10 (6) (2017 Dec) 886–894.
[49] L. Meng, D. Dong, X. Chen, M. Fang, R. Wang, J. Li, Z. Liu, J. Tian, 2D and 3D CT radiomic features performance comparison in characterization of gastric cancer: a multi-center study, IEEE J. Biomed. Health Inform. 25 (3) (2021 Mar) 755–763.
[50] L. Yang, J. Yang, X. Zhou, L. Huang, W. Zhao, T. Wang, J. Zhuang, J. Tian, Development of a radiomics nomogram based on the 2D and 3D CT features to predict the survival of non-small cell lung cancer patients, Eur. Radiol. 29 (5) (2019 May) 2196–2206.